Chemical Engineering Journal 466 (2023) 143146

Contents lists available at ScienceDirect

Chemical Engineering Journal

journal homepage: www.elsevier.com/locate/cej

Effective removal of nitrogen and phosphorus from a black-odorous water by novel oxygen-loaded adsorbents

Shu Xu [a,b], Jingfu Wang [a,c,*], Dengjun Wang [d], Peng Liao [a,c], Xinping Hu [a,c], Yongqiong Yang [b], Jingan Chen [a,c]

[a] State Key Laboratory of Environmental Geochemistry, Institute of Geochemistry, Chinese Academy of Sciences, Guiyang 550081, PR China
[b] School of Geography and Environmental Sciences, Guizhou Normal University, Guiyang 550025, PR China
[c] University of Chinese Academy of Sciences, Beijing 100049, PR China
[d] School of Fisheries, Aquaculture and Aquatic Sciences, Auburn University, Auburn, AL 36849, USA

ARTICLE INFO

Keywords:
Black-odorous water
Oxygen-loaded adsorbents
Phosphorus and Nitrogen removal
Oxygenation
Sediment

ABSTRACT

Black-odorous water, caused by hypoxia and overloading of nitrogen and phosphorus, is ubiquitous in global urban rivers. In this study, we developed oxygen-loaded adsorbents by loading oxygen into activated carbon, Attapulgite, Phoslock, and Muscovite via vacuum-pressure swing method, and investigated their aeration and removal efficiency of phosphate, ammonia nitrogen, and total nitrogen in black-odorous water. Results showed that the addition of oxygen-loaded coal-based columnar activated carbon (OCC) or oxygen-loaded Muscovite (OM) alone could increase the dissolved oxygen (DO) concentration at the sediment–water interface to more than 6 $mg{\cdot}L^{-1}$ on the first day, and OCC could maintain the high level of oxidation–reduction potential (ORP) (up to + 327 mV) for 15 days. Most oxygen-loaded adsorbents remarkably reduced phosphate in water, essentially from 0.27 $mg{\cdot}L^{-1}$ to < 0.05 $mg{\cdot}L^{-1}$. Additionally, ammonia nitrogen and total nitrogen were reduced by more than 50 % by adding materials after oxygen loading treatment. The 16 s RNA results showed that *Dechloromonas* was dominant in abundance, and the reduction of nitrogen was mainly affected by microbial activity. Our results provided a series of oxygen-loaded adsorbent materials with potential engineering applications for rapid treatment of urban black-odorous water.

1. Introduction

Black-odorous water is an extreme manifestation of organic pollution beyond its self-purification capacity in water environment. The word "black and odorous" is a sensory description of polluted water bodies. It refers to the devastating damage to urban ecology caused by black and odorous water bodies due to pollution, which is negatively impacting our daily life [1]. In China, the evaluation indexes of black-odorous water classification mainly include transparency, dissolved oxygen (DO), redox potential, and ammonia nitrogen[2]. The number of black-odorous water in China has increased to more than 2,100 by 2019 based on China urban black-odorous water treatment supervision platform[3].

Sediment is an important internal source of black-odorous water [4] because pollutants can accumulate in sediments through deposition, and physicochemical and biological adsorption [5]. Temperature rise, water disturbance or redox potential variation can cause pollutants to desorb from sediments and diffuse into surrounding water. Therefore, sediments not only act as a sink to concentrate pollutants deposited and adsorbed by water bodies [6], but also serve as sources to release pollutants into water bodies under low oxygen or disturbed environmental conditions, posing secondary pollution of water bodies [7]. In addition, the pollution released from sediment is a continuous process. Even after removing the external water pollution sources, the pollutants released from the sediment will reduce the effect of water pollution control. To this end, sediments as an important source of pollution must be given sufficient attention in the treatment of black-odorous water [8–10].

Due to the continuous accumulation of various pollutants in urban rivers, a large number of reducing substances in water and sediment lead to a rapid decline in DO (i.e., DO < 2 $mg{\cdot}L^{-1}$), which may eventually lead to black and odor. Low DO content inhibits the growth of aquatic organisms and further induces the death of these organisms[11], which continuously deteriorated the water quality. If the water oxygen level

* Corresponding author at: State Key Laboratory of Environmental Geochemistry, Institute of Geochemistry Chinese Academy of Sciences, Guiyang 550081, Guizhou Province, PR China.
E-mail address: wangjingfu@vip.skleg.cn (J. Wang).

https://doi.org/10.1016/j.cej.2023.143146
Received 21 February 2023; Received in revised form 19 April 2023; Accepted 20 April 2023
Available online 25 April 2023

cannot be improved, black-odorous water will bring many complex problems to aquatic ecosystems and human settlements [12].

To increase the DO content in water and reduce the nitrogen and phosphorus concentrations in water, several strategies have been developed, including artificial aeration, water cycle, chemical oxidation, microbial enhancement, and artificial floating island [1,13]. Among these, artificial aeration has the advantages of quick reaction, low cost, and environmental friendliness. It provides oxygen directly for the oxidation of reducing pollutants [2]. Traditional aeration approaches include blower aeration, mechanical stirring aeration, jet aeration, and mixed aeration. In the in-situ treatment technology, due to the oxygen transfer efficiency and oxygen retention capacity of the traditional aeration method, a large number of aerators are required to continuously supply oxygen, which leads to high energy consumption [1]. Moreover, aeration usually disturbs the water body, resulting the release of pollutants from sediments that may aggravate water pollution. Once the aeration is stopped, the DO drops rapidly to a low level, leading to the recurrence of water quality deterioration [14].

Under the anaerobic condition, the degradation of organic matter at the sediment–water interface (SWI) is often accompanied by the reduction of SO_4^{2-} [15], and excessive sulfides are generated in surface sediments. Sulfides combine with metal ions such as Fe^{2+} and Mn^{2+} to form metal sulfide complexes, resulting in the loss of binding sites of PO_4^{-}, which makes PO_4^{-} release from sediments to water [16–18]. Under aerobic conditions, DO can enhance the ammonification of organic N in overlying water, thereby promoting the transfer of N in sediments to bioavailable dissolved inorganic nitrogen. Secondly, the increase of DO and NH_4^+ during the ammonification process promoted aerobic nitrification, which transformed DIN from reducing NH_4^+ to nitrate N [19]. Nitrate can greatly promote the denitrification of deep sediments [20]. Therefore, considering the factors such as not disturbing the water body, it has become a new idea to control the release of N and P from sediments by precise oxygenation of the interface.

In this study, a black-odorous water column core simulation system was established in the laboratory. Oxygen was loaded into materials such as activated carbon, Phoslock and Muscovite by a vacuum-pressure swing [21]. These oxygen-loaded adsorbents were added to the sediment–water interface to test their efficiencies of oxygenation and contaminant removal. Planar optode (PO) [22] and diffusion gradient in thin films technology (DGT) [23] were used to characterize the dynamic changes of DO, phosphate, nitrogen, and sulfur concentrations at the sediment–water interface. This study aimed to: 1) evaluate the efficiency of oxygenation and nitrogen and phosphorus removal of different oxygen-loaded adsorbents in black-odorous water; and 2) explore the mechanism of nitrogen and phosphorus removal by those oxygen-loaded adsorption materials. It provides a theoretical basis for the emergency treatment of urban black and odorous water bodies by using a series of oxygen-carrying adsorption materials with potential engineering application value.

2. Materials and methods

2.1. Material preparation

The coal powder activated carbon, coal columnar activated carbon, and iron (Fe) modified activated carbon was purchased from Jiangsu Yiqing Activated Carbon Co., Ltd. The lanthanum (La)-modified Phoslock and La-modified attapulgite were provided by Beijing Fengslock Ecological Engineering Technology Co., Ltd. Muscovite (6,000 mesh) and Tuoyi New Materials (Guangzhou) Co., Ltd, respectively. Each of the above materials (2 ~ 3 g) is placed in a vacuum (-0.09 MPa) sealed container and degassed at room temperature (25 °C) for 2 h. After removing the air from the hole, pure oxygen gas was filled in the container and kept at a pressure of 0.8 MPa for 4 h to allow the diffusion of oxygen into the hole [21,24]. The oxygen-loaded adsorbents, including oxygen-loaded coal powder activated carbon (OPC), oxygen-loaded coal columnar activated carbon (OCC), oxygen-loaded iron modified activated carbon (OFeC), oxygen-loaded La modified Phoslock (OLP), oxygen-loaded La modified attapulgite (OLA), and oxygen-loaded Muscovite (OM), were stored before the experiment.

2.2. Material characterization

Scanning electron microscope (SEM, JSM7800F) was used to monitor the surface structure and determined the element composition of the synthesized materials. The particle size distribution of the material was measured by laser particle size analyzer (Mastersizer 2000, UK). The specific surface area and pore size distribution were measured by automatic specific surface and porosity analyzer BET (Micromeritics ASAP 2460, USA).

2.3. Sediment-water core culture tests

Fig. 1 showed the experimental schematic diagram. Surface sediments were collected from a black-odorous water in Guiyang, China, using a Peterson sampler. Water samples (20 L) were collected using a Niskin sampler to support the simulation experiment. Into the plastic bucket mixed evenly after static culture for 3 days to simulate stable black-odorous water. The 14 organic glass columns were divided into 7 groups, and these columns contained the same amount of sediment (height of about 5 cm) and water (depth of about 12 cm).

To investigate the effect of different materials on the removal of nitrogen and phosphorus in the cores, six groups of columns were covered on the surface of sediments with OPC, OCC, OFeC, OLP, OLA, and OM. Each group was tested in duplicates (n = 2). Two column cores without adding any material were used as blank control (BK). The culture experiment was conducted at 25 °C. Throughout the experiment, the column was wrapped in aluminum foils to avoid light.

During the incubation, the DO concentration at the sediment–water interface was measured daily using PO technology (EasySensor Ltd Co., Ltd., Nanjing, China). The PO oxygen film was cut into 2 cm × 4 cm strips and attached to the inner side of the organic glass box (8 cm × 8 cm × 20 cm) to observe the change of DO concentration at the sediment–water interface. The oxidation–reduction potential (ORP) of the sediment–water interface was measured by a multi-water quality parameter meter (YSI6600V2) every day. Fifty mL of overlying water was collected to determine the concentrations of soluble reactive phosphorus (SRP), ammonia nitrogen (NH_4^+-N), and total nitrogen (TN) on days 1, 2, 3, 5, 7, 10, 15, and 20. The concentration of SRP was determined by ammonium molybdate spectrophotometry [25]. Determination of NH_4^+-N concentration by Nessler's reagent spectrophotometry [26]. TN concentration was determined by high temperature digestion of alkaline potassium persulfate [27].

After each sampling, all test columns were gently supplied with raw water to compensate for the loss of water during sampling and evaporation. The AMP-TH & ZrO-Chelex DGT (Nanjing EasySensor Co., Ltd.) were used to determine the concentration of DGT-S (S^{2-}) and DGT-P (SRP) at the sediment–water interface. The DGT device penetrates the sediment core vertically without interfering with the sediment–water interface and undergoes a 24-hour equilibrium period before subsequent tests.

2.4. Microbial community analysis

To probe the potential mechanism of nitrogen removal of the oxygen-loaded adsorbents, the microbial community in the sediment was analyzed at the end of the cultivation experiment. Microbial communities in surface 2-cm sediments were collected. All samples were stored in a sterile centrifuge tube at − 80.0 °C until DNA extraction. Microbial DNA was extracted using a Qubit dsDNA HS analysis kit (ThermoFisher, Q32854, USA). The V3-V4 region of bacterial 16S rRNA gene was amplified by PCR using forward primer Nobar-341F

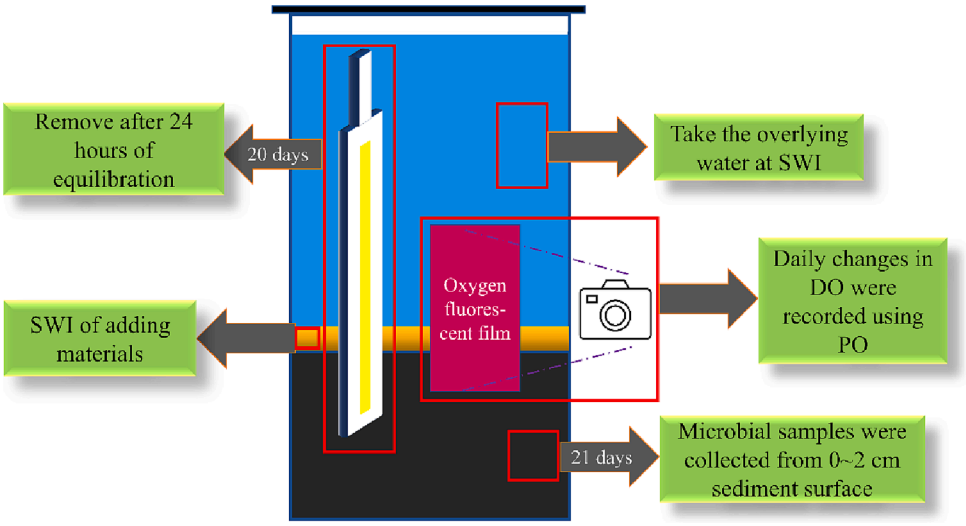

Fig. 1. Schematic diagram of experimental device, sampling and monitoring.

(CCTACGGNGGCWGCAG) and reverse primer Nobar-805R (GACTACHVGGGTATCTAATCC). Purified amplicons were pooled in equimolar amounts, and paired-end sequencing (2 × 300) was performed using the Illumina Miseq platform (Illumina, Sandiego, USA) according to the standard method recommended by Bioengineering Co., Ltd. (Shanghai, China).

2.5. Adsorption experiments

To evaluate the adsorption capacity of oxygen-loaded adsorbents, adsorption experiments were conducted with KH_2PO_4 (PO_4^+-P represents SRP) at 0.8 mg·L^{-1}, NH_4Cl (NH_4^+-N) at 30 mg·L^{-1}, and $NaNO_3$ (NO_3^--N) at 10 mg·L^{-1} as substrates. A 0.02 g of these oxygen-loaded adsorbents was added to 50 mL of KH_2PO_4, NH_4Cl, and $NaNO_3$ solutions. The concentration of SRP, NH_4^+-N, NO_3^--N in each group of water was measured at 1, 2, 3, 5, 7, 10, 15, 20, 30, 45, and 60 min after rotation at 25 °C. NO_3^--N was determined by phenol disulfonic acid ultraviolet spectrophotometry [26]. The pseudo-first-order kinetic model, pseudo-second-order kinetic model, Elovich model, and intraparticle diffusion model [28,29] were used to describe the adsorption mechanism.

3. Results

3.1. Characterization of synthesized materials

The particle size and specific surface area are distinctive between the substrate materials (Table 1). The maximum specific surface area of coal-based powder activated carbon is 1589.1 m^2·g^{-1}. The particle size of coal-based columnar activated carbon is higher than greater than 2 mm, with the specific surface area up to 1,000 m^2·g^{-1}. Muscovite has small particle size and uniform distribution, and its specific surface area is only 7.3 m^2·g^{-1}. It is interesting that small particle has low specific surface area due to the smooth two-dimensional structure of muscovite surface. Phoslock has a smaller particle size distribution than attapulgite, and the specific surface area of both is comparable. The specific surface area of OFeC is 251 m^2·g^{-1} due to the blocking of some voids by Fe_3O_4.

Table 1
Particle size distribution and BET surface area of substrate materials.

Name	d (0.1 μm)	d (0.5 μm)	d (0.9 μm)	BET (m^2·g^{-1})
Muscovite	1.7	4.5	8.8	7.3
Phoslock	2.0	11.5	35.8	12.4
Attapulgite	2.4	16.8	56.8	14.6
Fe modified carbon	1.6	16.9	61.0	251
Coal powder carbon	4.3	20.4	51.5	1,589
Coal columnar carbon	/	/	/	1,000

3.2. Variations of ORP, SRP, NH_4^+-N and TN in the overlying water

During the experiment, the ORP of overlying water in the BK treatment remained at a low level (<-300 mV, Fig. 2a). After adding OCC, the ORP of water was increased to + 327 mV. After 24 h, the ORP of overlying water treated with OPC, OCC, OFeC, OLP, OLA, and OM increased to about + 180 mV. Over time (greater than24 h), the ORP continued to decline. Among them, the ORP of water during OLP, OM and OLA treatments was decreased to near 0 mV in 10 days, while it took 15 days to achieve the same ORP (~0 mV) during activated carbon material treatments. Although the overlying water DO decreased rapidly within 5 days (Fig. 3), these oxygen-loaded adsorbents remarkably improved the ORP.

Throughout the experiment process, the SRP of the BK experiment was increased by 12.2% (Fig. 2b). The addition of oxygen-loaded adsorbents reduced the SRP concentration in the overlying water by nearly 90%, and reached equilibrium on day 10. On day 20, the SRP in the core water treated by OCC was the highest (0.07 mg·L^{-1}), while that treated by OFeC was only 0.03 mg·L^{-1}.

In the BK, the concentration of NH_4^+-N in the overlying water was maintained at about 32 mg·L^{-1} during the 20 days (Fig. 2c). The NH_4^+-N decreased sharply on the first day, followed by a rebound to the high values on day ~ 5, and then decreased slowly until reaching a plateau. In view of the absolute concentration of NH_4^+-N on day 20, the material with the highest removal efficiency was OLA, followed by OM.

In the BK, the TN in the overlying water reached the maximum (53.4 mg·L^{-1}) on day 7 (Fig. 2d). After adding the oxygen-loaded adsorbents, the variation of TN concentration was similar to that of NH_4^+-N. Compared with the BK, the TN concentration of the overlying water in all experimental groups was significantly decreased, and the lowest TN concentration was 22.2 mg·L^{-1} (decrease by 56%) in the cores treated with OM.

3.3. Variation of DO concentration at the sediment–water interface

The DO at the sediment–water interface in the BK remained at a low level (<0.1 mg·L^{-1}). After adding oxygen-loaded adsorbents, the DO concentration was increased rapidly on day 1 (Figs. 3 and 4). In cores

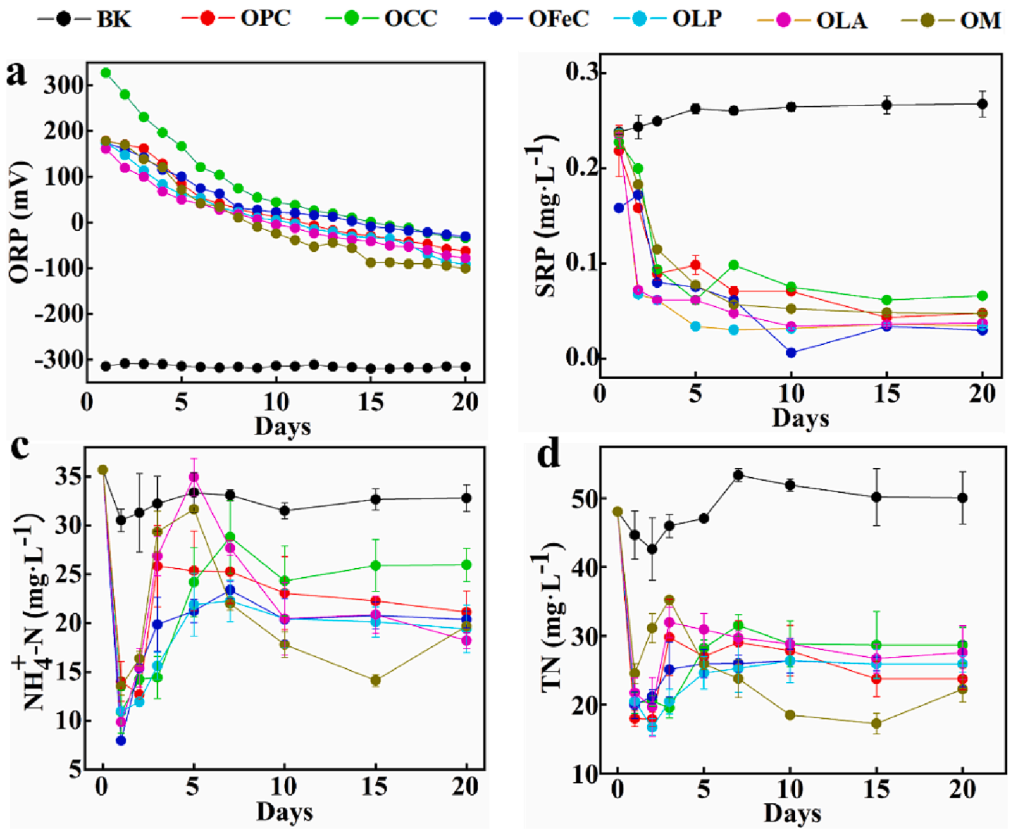

Fig. 2. Variations of ORP (a), SRP (b), NH_4^+-N (c), and TN (d) in the overlying water over 20 days of incubation. BK represents blank control, and OPC, OCC, OFeC, OLP, OLA, and OM represent different oxygen-loaded adsorbents.

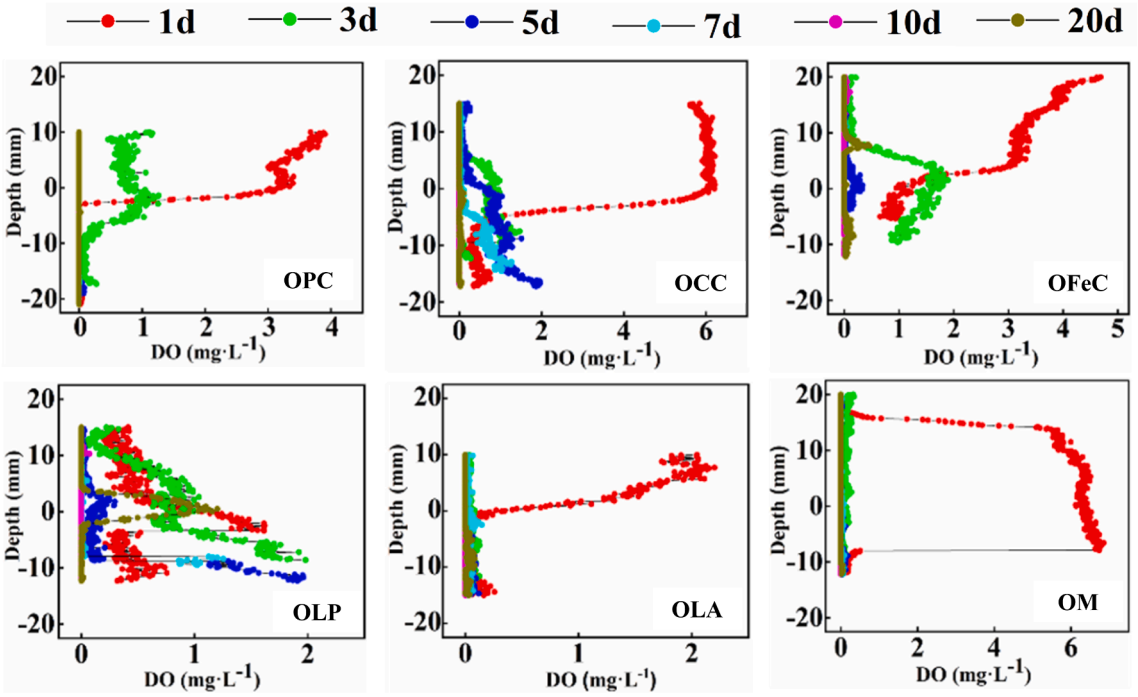

Fig. 3. The variation of DO at the sediment–water interface in cores treated various oxygen-loaded adsorbents with time (days 1, 3, 5, 10, and 20). Above the 0-tick mark indicates overlying water, and below indicates sediment.

treated by OLP, 2 mg·L^{-1} concentration of DO could still be detected in the sediment at a depth of 10 mm on day 5. The DO concentration also reached to 2 mg·L^{-1} in cores treated by OLA, but it only lasted for 1 day. The addition of OM increased the DO level at the sediment–water interface on the first day, reaching nearly 7 mg·L^{-1} and penetrating 10 mm in sediments. After day 1 of OPC addition, the DO was reached to 4

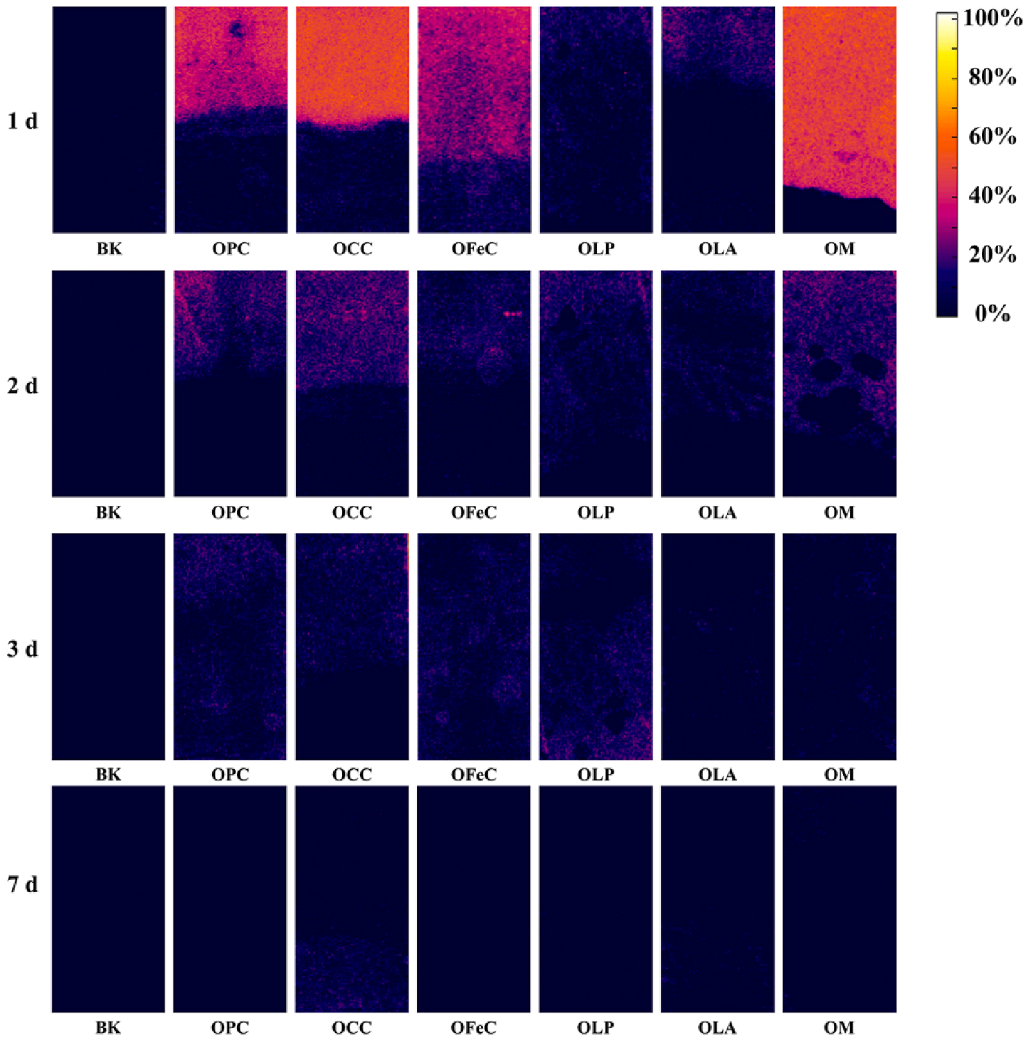

Fig. 4. The DO profiles at the sediment–water interface in cores of blank control and those treated by oxygen-loaded adsorbents within 7 days.

mg·L^{-1} and then decreased to 1 mg·L^{-1} on day 3. The oxygenation efficiency and holding time of OFeC were similar to OPC. After dosing, the DO in cores treated by OCC reached the level close to that of OM, and 1 mg·L^{-1} DO remained detected in the sediment at a depth of 10 mm on day 7 (Fig. 4).

The oxygenation time and permeability of different materials may be related to the shape and quality of the material. According to the naked eye observation, when OPC was added, it initially floated to the surface of the water and continued to release large bubbles (diameter greater than 1 mm), and then gradually sank to the bottom after about 20 s. In this process, a large amount of oxygen was released into the air, resulting in a loss of oxygen in the material, which may be related to the increased buoyancy caused by the excessive amount of oxygen loaded on the material.

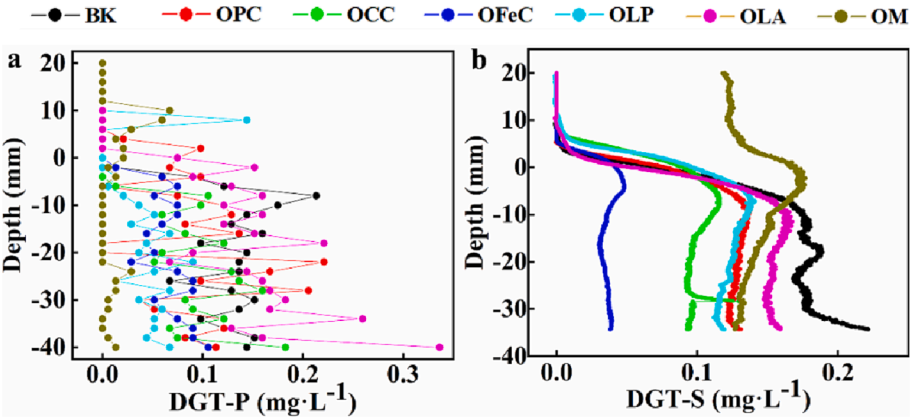

Fig. 5. One-dimensional plots of DGT-P (a) and DGT-S (b) in the experimental groups of blank control and dosing oxygen-loaded adsorbents.

3.4. Variation of DGT-P and DGT-S at the sediment–water interface

On day 20, the distribution of DGT-P in sediment profiles treated by varied oxygen-loaded adsorbents was remarkably different (Fig. 5a). The addition of OM has the most significant effect on the concentration gradient of DGT-P near the sediment–water interface, significantly reducing the release rate of phosphate from pore water to overlying water. The addition of OLA did not significantly inhibit the release of DGT-P in sediments. The distribution of DGT-P at the sediment–water interface of the column cores treated with OLA was similar to that of BK group. Other oxygen-loaded adsorbents also inhibited the release of DGT-P at the sediment–water interface, and their control efficiency on the release of phosphate in pore water placed between OM and LOA.

The concentration of DGT-S at the depth of 0 mm (about 0.05 mg·L^{-1}) in BK and cores added with OPC, OCC, OLP and OLA were close to each other (Fig. 5b). Compared with the BK, the DGT-S in 0–30 mm sediment treated with oxygen-loaded adsorbents decreased, among which cores treated with OFeC decreased most. The distribution of DGT-S in core sediments and overlying water with OM addition became uniform (Fig. 6). The DGT-S concentration of the column cores with OM addition was about 0.17 mg·L^{-1}.

3.5. Effect of oxygen-loaded adsorbents on microbial community in surface sediment

Fig. 7a showed the microbial community composition (phylum level) in the sediments of different treatments on day 20. The dominant species in cores treated by various oxygen-loaded adsorbents were similar, including *Chloroflexi, Proteus* and *Bacteroides*. The relative abundance of *Chloroflexi* and *Proteobacteria* in core sediment of BK and that treated by OFeC was similar, while *Bacteroides* in core sediment added with OFeC was slightly higher than that in BK. The relative abundance of *Proteobacteria* in core sediments added with OCC, OPC, OLP, OLA and OM were less than that in BK, while the relative abundance of *Chloroflexi* and *Bacteroides* was much higher than that in BK.

The related microorganisms were further investigated at the genus level (Fig. 7b). *Dechloromonas* were predominant in all groups, but the relative abundance in the core sediments added with materials (OCC:77%, OPC:75%, OFeC:74%, OLP:75%, OLA:76% and OM:73%) was higher than that in the BK (68%). *Longilinea* and *Thermomonas* had the highest relative abundances in the BK, with 8% and 12% respectively, and their abundance ratios in the core sediments added with the oxygen-loaded adsorbents decreased slightly. The relative abundance of *Gemmobacter* in the core sediments added with the oxygen-loaded adsorbents was slightly higher than that in the BK.

3.6. Adsorption efficiency of oxygen-loaded adsorbents for nitrogen and phosphorus in simulated sediment–water system

The adsorption of SRP, NH_4^+-N, and NO_3^--N by all oxygen-loaded adsorbents occurred almost within a few minutes. Although the adsorption of OM on SRP showed a trend of fluctuation (Fig. 8a), compared with 0 min, OM did not adsorb SRP at 60 min. The adsorption of SRP by OCC, OPC and OLA reached adsorption equilibrium within 1 min, and the removal rate was about 29%. OLP and OFeC exhibited high adsorption for SRP. At 60 min, the adsorption efficiency of OFeC and OLP was higher than 96%.

All materials showed similar adsorption behavior for NH_4^+-N (Fig. 8b). The highest removal efficiency of NH_4^+-N by OLA was 35.7% within the first 7 min. The removal efficiency of NH_4^+-N by OLA was only 14.3% in the 60 min. The lowest adsorption efficiency of NH_4^+-N was OLP (5.8%). The adsorption efficiency of nitrate nitrogen by OLP was 18.2. OPC and OM had high adsorption efficiency of nitrate nitrogen, with 33.5% and 32.8% respectively (Fig. 8c).

To reveal the adsorption mechanism of OFeC and OLP on SRP in water and determine the adsorption rate of the materials, the pseudo-first-order kinetic model, pseudo-second-order kinetic model, Elovich kinetic model and intraparticle diffusion model were further used to fit the experimental data. The fitting results were shown in Fig. 6 and Table 2. Clearly the pseudo-first-order kinetic model (OFeC: $R^2 = 0.973$; OLP: $R^2 = 0.971$), and Elovich kinetic model (OFeC: $R^2 = 0.917$; OLP: $R^2 = 0.754$) were more suitable for describing the adsorption kinetics of SRP in water by OFeC and OLP. The k_1 of OFeC fitted by the pseudo-first-order kinetic equation model in Table 2 is larger than that of OLP, indicating that OFeC is faster in the initial stage of adsorption, which can also be seen from the curve in Fig. 8d. To confirm whether the rate-limiting step of OFeC and OLP adsorbing phosphate in water is intraparticle diffusion or membrane diffusion, the experimental data were further fitted by the intraparticle diffusion model. According to the relationship between q_t and $t^{0.5}$, all data do not pass the origin, indicating that intraparticle diffusion is not the rate-limiting step in the adsorption reaction process [30,31].

The pseudo-first-order kinetic model was used to describe the physical adsorption kinetic process, and the Elovich kinetic model was used to describe the chemical adsorption kinetic process. The fitted results showed that the main mechanism of SRP adsorption by OFeC and

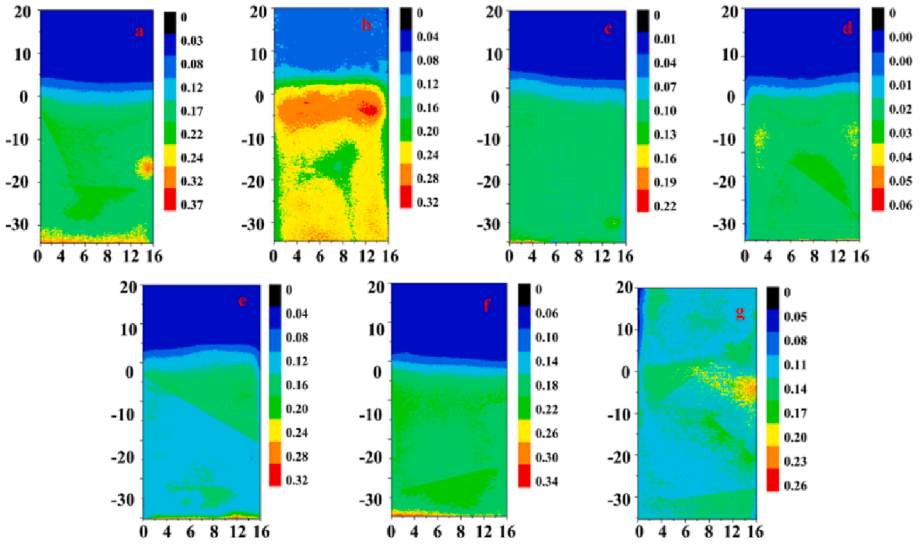

Fig. 6. Two-dimensional distribution of DGT-S in cores of blank control (a), OPC (b), OCC (c), OFec (d), OLP (e), OLA (f) and OM (g) on the day 20.

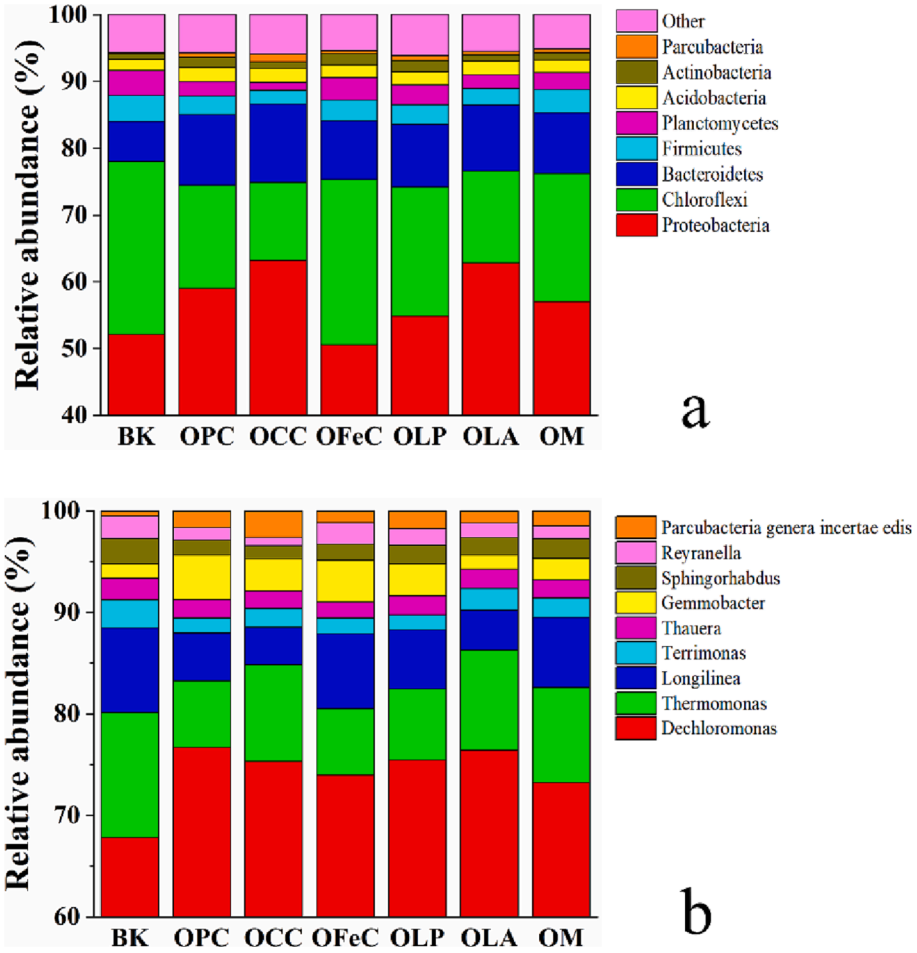

Fig. 7. Microbial species abundance at the phylum level (a) and genus level (b) in the surface 0–2 cm sediments.

OLP was physical adsorption. When describing the adsorption process of OFeC and OLP, the fitting of pseudo-first-order kinetic model was better than that of pseudo-second-order kinetic model (Fig. 8 and Table 2), indicating that physical adsorption was the rate-limiting step of SRP adsorption[32].

4. Discussion

4.1. The physical properties of the adsorbents determine their oxygen load and nutrient adsorption capacity

Current methods using H_2O_2, CaO, and mechanical aeration for improving DO levels in the water environment, can cause sediment disturbance leading to secondary release of pollutants [21], the method of loading oxygen porous materials appears to be more advantageous [24]. In this study, we found that the surface microstructure, specific surface area, and particle size distribution of porous materials were related to the oxygen carrying capacity. The rougher the surface microstructure, the larger the specific surface area, and the slower the oxygen release (Figs. 3, 4 and Table 1). Muscovite is a smooth planar structure with a small specific surface area and is quickly consumed in the process of releasing oxygen. Although the specific surface area of OLP and OLA is close to that of OM, the uneven surface is more conducive to the slow release of oxygen (Fig. 1and 3). Therefore, the specific surface area of OCC and OPC is higher than that of OLA, OLP and OM, which helps to improve the oxygen loading capacity. Although the specific surface area of OPC is larger than that of OCC, its particle size is much smaller than that of OCC. The contact area between oxygen and water molecules loaded by OCC during sedimentation is larger than that of OPC, which results in a higher oxygen release rate of OCC than OPC. After the oxygen on the surface of OCC is released, the internal oxygen is slowly dissolved in water, which may be the reason why OCC exceeds other materials in oxygenation duration.

In addition to loading oxygen, these oxygen-loaded adsorbents also have high adsorption capacity for nitrate, ammonia and phosphate. Documented studies have used adsorption and passivation materials, such as activated carbon, clay and lanthanum modified bentonite, to reduce the release of nutrients inside the sediment [33]. To achieve sufficient internal nutrient reduction, oxygen nanobubbles modified porous materials have also been applied at the microcosmic scale [34]. Depending on the initial nutrient concentration and DO level, different adsorption passivation materials can control the release of internal nutrients. The adsorption experimental results showed that the adsorption of phosphate on OFeC and OLP was high (Fig. 8). Although the adsorption of phosphate by OM was also adsorbed at the beginning, the phosphate was released again in the subsequent oscillation process. Lanthanum has a high affinity for phosphates[35] and was therefore widely used to modify clays or porous materials to enhance phosphate removal [36]. Under aerobic conditions, some sediments can form stable cyanite and strongly fix phosphate [37]. Similarly, in our adsorption experiments, OFeC and OLP strongly adsorb phosphate because they contain a high content of oxidized Fe (Fig. 8a).

In eutrophic lakes, ORP in the surface sediment profile usually decreases rapidly with depth, resulting in the simultaneous release of NH_4^+-N and phosphate [36,38]. In this study, the oxygen-carrying adsorbent not only rapidly increased the ORP in the water column, but also the material itself penetrated into the sediment, improved the DO and ORP levels in the surface sediment, thereby improving the adsorption

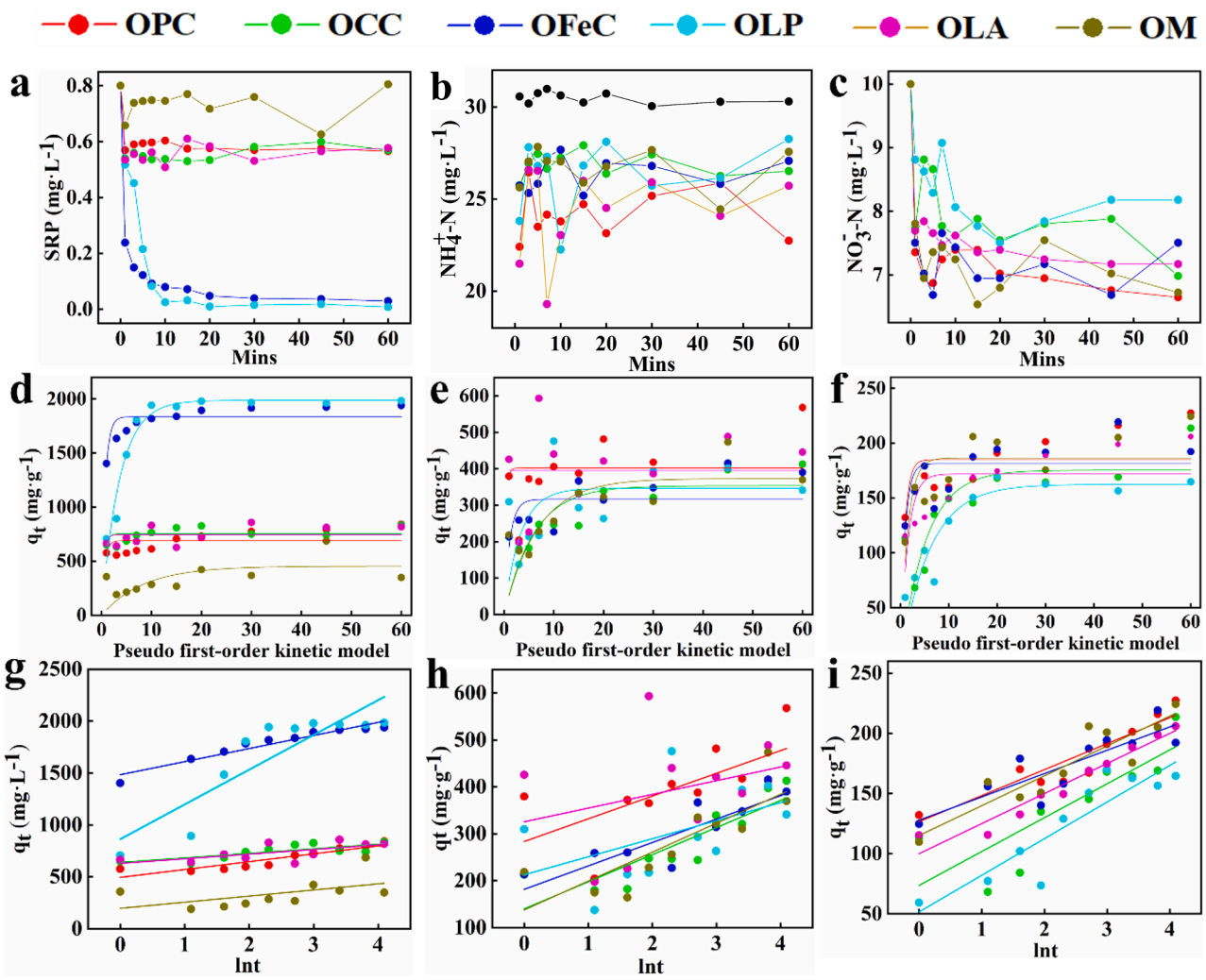

Fig. 8. The adsorption of SRP (a), NH_4^+-N (b), and NO_3^-–N (c) in the solution by adding various materials within 60 min. SRP (d), (NH_4^+-N (e), and NO_3^--N (f) represent the pseudo first-order kinetic model fitted results. SRP (g), NH_4^+-N (h), and NO_3^--N (i) represent the Elovich kinetic model fitted results. q_t refers to the adsorption capacity.

Table 2
Kinetic parameters and correlation coefficients of SRP adsorption on OFeC and OLP.

Models	Parameters	OFeC	OLP
Pseudo first-order kinetic model	q_e (mg·g^{-1})	1,835	1,987
	k_1 (1/min)	1.37	0.278
	R^2	0.973	0.971
Pseudo second-order kinetic model	q_e (mg·g^{-1})	360	342
	k_2 (1/min)	0.002	0.004
	R^2	0.940	0.892
Elovich	a (mg·g^{-1})b	1,483	863
	(1/min)	126	335
	R^2	0.917	0.754
Intraparticle Diffusion	K_{i1} (mg·g^{-1})C	1,378	−7.14
	(1/min)	127	637
	R^2	0.829	0.920
	K_{i2} (mg·g^{-1})C	1,840	1,916
	(1/min)	12.8	8.52
	R^2	0.931	0.358

capacity of the material itself and the sediment to nitrogen and phosphorus pollutants, while inhibited the diffusion of nitrogen and phosphorus from the sediment to the overlying water.

4.2. Oxygen loading is beneficial to the biological removal of nitrogen and phosphorus in black-odorous water

In natural water, the transport and transformation of nitrogen and phosphorus are mainly controlled by microbial processes in addition to physical and chemical adsorption [24]. For example, nitrification and denitrification can convert nitrogen into multiple forms in water [39]. In this study, the concentration of NH_4^+-N in the overlying water increased initially but then decreased, and the removal rate of NH_4^+-N in the overlying water with different materials was significantly different (Fig. 2c). The concentration of NH_4^+-N in the overlying water of OM treatment was significantly lower than that of other treatments on day 15, which may be related to the decrease of ORP to negative value after Muscovite oxygen release. The concentration of NH_4^+-N in OCC treatment was higher than that in other treatment groups on day 20, which may be related to the continuous release of oxygen by OCC, the later decrease of ORP to negative value and the later dominant time of denitrification. The effect of elevated concentrations of NH_4^+-N by dissimilatory nitrate reduction in overlying water cannot be ruled out here [40]. This process is carried out through a chemical autotrophic pathway using sulfides as electron donors [41,42]. The sediments were rich in reduced sulfur (Fig. 5b and 6), which was likely to be one reason why the NH_4^+-N concentration did not continue to decline.

Nitrification is responsible for converting NH_4^+-N to NO_3^--N, rather

than eliminating N from aquatic systems [43]. In aquatic ecosystems, denitrification is an important way to reduce nitrogen, and nitrification is often accompanied by denitrification [44]. It should be noted that the concentration of nitrate nitrogen and ammonia nitrogen in the overlying water decreased significantly in the experiment (Fig. 3c, d), suggesting the occurrence of denitrification or biological assimilation. Microbial analysis confirmed that dechlorinating bacteria are ubiquitous in surface sediments [45], which is conducive to denitrification and phosphorus removal, reducing SRP and NO_3^--N in anaerobic environments (Fig. 6b). Therefore, it can be concluded that the reduction of nitrate nitrogen and NH_4^+-N in the cores was related to the proliferation of denitrifying bacteria and the subsequent denitrification process[24].

Although the oxygenation duration of these materials was only maintained for 7 days, it still affected the microbial cycle of nitrogen. The concentration of NH_4^+-N generally reached the maximum value on day 5 after the addition of the material. This is likely because the addition of the material increases the DO of the water body and promotes the ammonification process, leading to the increase of NH_4^+-N concentration. When the oxygen was consumed, the water returned to the anaerobic state, and the denitrification led to the removal of NH_4^+-N and TN. After 20 days, DO cannot be detected in the cores, and microorganisms such as Bacillus maintained a high abundance. *Gemmobacter* is an anaerobic denitrifying bacterium [46]. After 20 days, the abundance of *Gemmobacter* was slightly higher than that of BK, indicating that oxygen content affected the microbial cycle process in the early oxygenation process and the later anaerobic process. This phenomenon was also reported in intermittent microaerobic aeration [47].

5. Conclusion

This study proposed a cost-effective method to achieve oxygenation and nitrogen and phosphorus removal from a black-odorous water. Several oxygen-loaded adsorbents were synthesized by loading oxygen into activated carbon, passivator, and Muscovite. These oxygen-loaded adsorbents can remarkably increase the DO level at the sediment–-water interface, and greatly increase the ORP (keep above 0 mV for 15 days) in the overlying water. Meanwhile, oxygen-loaded adsorbents decreased the concentrations of SRP, NH_4^+-N and TN in the water bodies by the physical adsorption, along with microbial participation. Among these materials, OFeC and OLP showed high adsorption efficiency for phosphate. The addition of oxygen-loaded adsorbents changed the sediment microbial community and promoted the abundance of nitrifying and denitrifying bacteria. Based on the results of oxygenation, OFeC and OLP are more suitable for phosphorus and nitrogen inhibition among these materials. Improving the gas-carrying capacity of the materials and the aging of the oxygen-loaded adsorbents are the key strategies that need to be improved in the future. These newly developed materials could simultaneously realize the oxygenation and pollutant removal, showing an optimistic application prospect in the treatment of black odor problem in urban rivers.

Declaration of Competing Interest

The authors declare that they have no known competing financial interests or personal relationships that could have appeared to influence the work reported in this paper.

Data availability

Data will be made available on request.

Acknowledgements

This study was sponsored jointly by the National Key R&D Plan of China (No. 2021YFC3201000), the Guizhou Science and Technology Plan Project ([2020] 4Y006), the Stratiogic Priority Research Program of CAS (No. XDB40020400), the Chinese NSF project (No. 41977296, 42277253), the Central Leading Local Science and Technology Development Fund Project (No. 20214028), the Guizhou Provincial 2019 Science and Technology Subsidies (No. GZ2019SIG), and the Youth Innovation Promotion Association CAS (No. 2019389).

Ethical Approval Not applicable.

Consent to Participate Not applicable.

Consent to Publish Not applicable.

Authors contributions **Shu Xu** and **Jingfu Wang** contributed to the conception and design of this study. **Shu Xu** and **Xinping Hu** collated the database and performed statistical analysis. **Shu Xu** wrote the first draft of the manuscript. **Jingfu Wang**, **Dengjun Wang**, **Peng Liao, Yongqiong Yang** and **Jingan Chen** guided the writing of the thesis. All authors have read and agreed to the published version of the manuscript.

Availability of data and materials The authors confirm that the data supporting the findings of this study are available within the article and its supplementary materials.

References

[1] J.X. Cao, Q. Sun, D.H. Zhao, M.Y. Xu, Q.S. Shen, D. Wang, Y. Wang, S.M. Ding, A critical review of the appearance of black-odorous waterbodies in China and treatment methods, J. Hazard. Mater. 385 (2020) 18, https://doi.org/10.1016/j.jhazmat.2019.121511.

[2] H.B. Yin, J.F. Wang, R.Y. Zhang, W.Y. Tang, Performance of physical and chemical methods in the co-reduction of internal phosphorus and nitrogen loading from the sediment of a black odorous river, Sci. Total Environ. 663 (2019) 68–77, https://doi.org/10.1016/j.scitotenv.2019.01.326.

[3] Y.E. Liu, X.J. Luo, C.C. Huang, Y.H. Zeng, Q.H. Lu, S.Q. Wang, B.X. Mai, Legacy and alternative plasticizers in surface sediment of black-odorous urban rivers across China: Occurrence, spatial distribution, and ecological risk assessment, Chemosphere 283 (2021) 8, https://doi.org/10.1016/j.chemosphere.2021.131206.

[4] J. Chen, P. Xie, Z.M. Ma, Y.A. Niu, M. Tao, X.W. Deng, Q. Wang, A systematic study on spatial and seasonal patterns of eight taste and odor compounds with relation to various biotic and abiotic parameters in Gonghu Bay of Lake Taihu, China, Sci. Total Environ. 409 (2) (2010) 314–325, https://doi.org/10.1016/j.scitotenv.2010.10.010.

[5] K.D. Bastami, H. Bagheri, V. Kheirabadi, G.G. Zaferani, M.B. Teymori, A. Hamzehpoor, F. Soltani, S. Haghparast, S.R.M. Harami, N.F. Ghorghani, S. Ganji, Distribution and ecological risk assessment of heavy metals in surface sediments along southeast coast of the Caspian Sea, Mar. Pollut. Bull. 81 (1) (2014) 262–267, https://doi.org/10.1016/j.marpolbul.2014.01.029.

[6] A. Karimi, S. Abdollahi, K. Ostad-Ali-Askari, S. Eslamian, V. P. Singh, Predicting fire hazard areas using vegetation indexes, Case Study: Forests of Golestan province, Iran, J. Geograp. Cartograp. 4(1) (2021). 10.24294/jgc.v4i1.451.

[7] Y.Y. Zhuang, H.E. Allen, G.M. Fu, EFFECT OF AERATION OF SEDIMENT ON CADMIUM-BINDING, Environ. Toxicol. Chem. 13 (5) (1994) 717–724, https://doi.org/10.1002/etc.5620130505.

[8] M. Varol, B. Sen, Assessment of nutrient and heavy metal contamination in surface water and sediments of the upper Tigris River, Turkey, Catena 92 (2012) 1–10, https://doi.org/10.1016/j.catena.2011.11.011.

[9] H. Li, C.L. Song, L. Yang, H.D. Qin, X.Y. Cao, Y.Y. Zhou, Phosphorus supply pathways and mechanisms in shallow lakes with different regime, Water Res. 193 (2021) 13, https://doi.org/10.1016/j.watres.2021.116886.

[10] Y.T. Wang, T.Q. Zhang, Y.C. Zhao, J.J.H. Ciborowski, Y.M. Zhao, I.P. O'Halloran, Z.M. Qi, C.S. Tan, Characterization of sedimentary phosphorus in Lake Erie and on-site quantification of internal phosphorus loading, Water Res. 188 (2021) 10, https://doi.org/10.1016/j.watres.2020.116525.

[11] J. Ruiz-Sanchez, M. Guivernau, B. Fernandez, J. Vila, M. Vinas, V. Riau, F. X. Prenafeta-Boldu, Functional biodiversity and plasticity of methanogenic biomass from a full-scale mesophilic anaerobic digester treating nitrogen-rich agricultural wastes, Sci Total Environ 649 (2019) 760–769, https://doi.org/10.1016/j.scitotenv.2018.08.165.

[12] K.T. Lu, H.J. Gao, H.B. Yu, D.P. Liu, N.M. Zhu, K.L. Wan, Insight into variations of DOM fractions in different latitudinal rural black-odor waterbodies of eastern China using fluorescence spectros-copy coupled with structure equation model, Sci. Total Environ. 816 (2022) 11, https://doi.org/10.1016/j.scitotenv.2021.151531.

[13] F. Shi, Z.L. Liu, J.L. Li, H.W. Gao, S. Qin, J.J. Guo, Alterations in microbial community during the remediation of a black-odorous stream by acclimated composite microorganisms, J. Environ. Sci. 118 (2022) 181–193, https://doi.org/10.1016/j.jes.2021.12.034.

[14] W.H. Wang, Y. Wang, J.J. Li, H. Zhang, F.L. Yan, L.Q. Sun, Dose effects of calcium peroxide on harmful gases emissions in the anoxic/anaerobic landscape water system, Environ. Pollut. 255 (2019) 10, https://doi.org/10.1016/j.envpol.2019.112989.

[15] S. Thodeandersen, B.B. Jorgensen, SULFATE REDUCTION AND THE FORMATION OF S-35-LABELED FES, FES2, AND S0 IN COASTAL MARINE-SEDIMENTS, Limnol. Oceanogr. 34 (5) (1989) 793–806, https://doi.org/10.4319/lo.1989.34.5.0793.

[16] C.M. Swarzenski, T.W. Doyle, B. Fry, T.G. Hargis, Biogeochemical response of organic-rich freshwater marshes in the Louisiana delta plain to chronic river water influx, Biogeochemistry 90 (1) (2008) 49–63, https://doi.org/10.1007/s10533-008-9230-7.
[17] F. Sulu-Gambari, D. Seitaj, F.J.R. Meysman, R. Schauer, L. Polerecky, C.P. Slomp, Cable Bacteria Control Iron-Phosphorus Dynamics in Sediments of a Coastal Hypoxic Basin, Environ. Sci. Technol. 50 (3) (2016) 1227–1233, https://doi.org/10.1021/acs.est.5b04369.
[18] A. Picard, A. Gartman, J. Cosmidis, M. Obst, C. Vidoudez, D.R. Clarke, P.R. Girguis, Authigenic metastable iron sulfide minerals preserve microbial organic carbon in anoxic environments, Chem. Geol. 530 (2019) 13, https://doi.org/10.1016/j.chemgeo.2019.119343.
[19] M. Liu, Y.X. He, L. Cao, Y. Zhi, X.J. He, T. Li, Y.Y. Wei, X.B. Yuan, B.S. Liu, Q. He, H. Li, X.J. Miao, Fate of dissolved inorganic nitrogen in turbulent rivers: The critical role of dissolved oxygen levels, Environ. Pollut. 312 (2022) 11, https://doi.org/10.1016/j.envpol.2022.120074.
[20] Y.J. Li, H.Y. Jin, J.F. Chen, D.Q. Wang, Z. Yang, B. Wang, Y.P. Zhuang, R. Wang, Nitrogen removal through sediment denitrification in the Yangtze Estuary and its adjacent East China Sea: A nitrate limited process during summertime, Sci. Total Environ. 795 (2021) 10, https://doi.org/10.1016/j.scitotenv.2021.148616.
[21] M. Liu, Y. Ran, X.X. Peng, Z.Q. Zhu, J.L. Liang, H.N. Ai, H. Li, Q. He, Sustainable modulation of anaerobic malodorous black water: The interactive effect of oxygen-loaded porous material and submerged macrophyte, Water Res. 160 (2019) 70–80, https://doi.org/10.1016/j.watres.2019.05.045.
[22] R.N. Glud, C.M. Santegoeds, D. De Beer, O. Kohls, N.B. Ramsing, Oxygen dynamics at the base of a biofilm studied with planar optodes, Aquat. Microb. Ecol. 14 (3) (1998) 223–233, https://doi.org/10.3354/ame014223.
[23] S.M. Ding, C. Han, Y.P. Wang, L. Yao, Y. Wang, D. Xu, Q. Sun, P.N. Williams, C. S. Zhang, In situ, high-resolution imaging of labile phosphorus in sediments of a large eutrophic lake, Water Res. 74 (2015) 100–109, https://doi.org/10.1016/j.watres.2015.02.008.
[24] G.N. Wei, R.Y. Yuan, M. Salam, L.X. Zhang, Y.Y. Wei, B.R. Tang, X.B. Yuan, B. S. Liu, X.H. Yu, H. Li, X.J. Miao, Achieving simultaneous removal of nitrogen and phosphorus in sediment via combined adsorption and oxygen supplement, Chem. Eng. J. 441 (2022) 11, https://doi.org/10.1016/j.cej.2022.136056.
[25] J. Murphy, J.P. Riley, CITATION-CLASSIC - A MODIFIED SINGLE SOLUTION METHOD FOR THE DETERMINATION OF PHOSPHATE IN NATURAL-WATERS, Curr. Contents/Agricult. Biol. Environ. Sci. (12) (1986) 16-16.
[26] X.H. Xia, Z.F. Yang, X.Q. Zhang, Effect of Suspended-Sediment Concentration on Nitrification in River Water: Importance of Suspended Sediment-Water Interface, Environ. Sci. Technol. 43 (10) (2009) 3681–3687, https://doi.org/10.1021/es8036675.
[27] C.H. Yang, P. Yang, J. Geng, H.B. Yin, K.N. Chen, Sediment internal nutrient loading in the most polluted area of a shallow eutrophic lake (Lake Chaohu, China) and its contribution to lake eutrophication, Environ. Pollut. 262 (2020) 10, https://doi.org/10.1016/j.envpol.2020.114292.
[28] S. Azizian, Kinetic models of sorption: a theoretical analysis, J. Colloid Interface Sci. 276 (1) (2004) 47–52, https://doi.org/10.1016/j.jcis.2004.03.048.
[29] Y.S. Ho, Review of second-order models for adsorption systems, J. Hazard. Mater. 136 (3) (2006) 681–689, https://doi.org/10.1016/j.jhazmat.2005.12.043.
[30] Z.G. Ren, F. Chen, B. Wang, Z.X. Song, Z.Y. Zhou, D. Ren, Magnetic biochar from alkali-activated rice straw for removal of rhodamine B from aqueous solution, Environ. Eng. Res. 25 (4) (2020) 536–544, https://doi.org/10.4491/eer.2019.232.
[31] A. Hamid, A.E. Wilson, H.A. Torbert, D. Wang, Sorptive removal of phosphorus by flue gas desulfurization gypsum in batch and column systems, Chemosphere (2023), 138062, https://doi.org/10.1016/j.chemosphere.2023.138062.
[32] J.F. Yu, H.P. Feng, L. Tang, Y. Pang, J.J. Wang, J.J. Zou, Q.Q. Xie, Y.N. Liu, C. Y. Feng, J.J. Wang, Insight into the key factors in fast adsorption of organic pollutants by hierarchical porous biochar, J. Hazard. Mater. 403 (2021) 10, https://doi.org/10.1016/j.jhazmat.2020.123610.
[33] Y. Tang, M.Y. Zhang, J. Zhang, T. Lyu, M. Cooper, G. Pan, Reducing arsenic toxicity using the interfacial oxygen nanobubble technology for sediment remediation, Water Res. 205 (2021) 10, https://doi.org/10.1016/j.watres.2021.117657.
[34] U. Kamran, S.J. Park, Microwave-assisted acid functionalized carbon nanofibers decorated with Mn doped TNTs nanocomposites: Efficient contenders for lithium adsorption and recovery from aqueous media, J. Ind. Eng. Chem. 92 (2020) 263–277, https://doi.org/10.1016/j.jiec.2020.09.014.
[35] X.D. Li, Q. Xie, S.H. Chen, M.C. Xing, T. Guan, D.Y. Wu, Inactivation of phosphorus in the sediment of the Lake Taihu by lanthanum modified zeolite using laboratory studies, Environ. Pollut. 247 (2019) 9–17, https://doi.org/10.1016/j.envpol.2019.01.008.
[36] M. Hupfer, S. Jordan, C. Herzog, C. Ebeling, R. Ladwig, M. Rothe, J. Lewandowski, Chironomid larvae enhance phosphorus burial in lake sediments: Insights from long-term and short-term experiments, Sci. Total Environ. 663 (2019) 254–264, https://doi.org/10.1016/j.scitotenv.2019.01.274.
[37] H.Z. Yuan, H.X. Wang, Y.W. Zhou, B.C. Jia, J.H. Yu, Y.W. Cai, Z. Yang, E.F. Liu, Q. Li, H.B. Yin, Water-level fluctuations regulate the availability and diffusion kinetics process of phosphorus at lake water-sediment interface, Water Res. 200 (2021) 15, https://doi.org/10.1016/j.watres.2021.117258.
[38] G. Pan, L.C. Dai, L. Li, L.C. He, H. Li, L. Bi, R.D. Gulati, Reducing the Recruitment of Sedimented Algae and Nutrient Release into the Overlying Water Using Modified Soil/Sand Flocculation-Capping in Eutrophic Lakes, Environ. Sci. Technol. 46 (9) (2012) 5077–5084, https://doi.org/10.1021/es3000307.
[39] D. Negi, S. Verma, S. Singh, A. Daverey, J.G. Lin, Nitrogen removal via anammox process in constructed wetland - A comprehensive review, Chem. Eng. J. 437 (2022) 13, https://doi.org/10.1016/j.cej.2022.135434.
[40] F.Y. Deng, L.J. Hou, M. Liu, Y.L. Zheng, G.Y. Yin, X.F. Li, X.B. Lin, F. Chen, J. Gao, X.F. Jiang, Dissimilatory nitrate reduction processes and associated contribution to nitrogen removal in sediments of the Yangtze Estuary, J. Geophys. Res.-Biogeosci. 120 (8) (2015) 1521–1531, https://doi.org/10.1002/2015jg003007.
[41] R.C. Brunet, L.J. GarciaGil, Sulfide-induced dissimilatory nitrate reduction to ammonia in anaerobic freshwater sediments, FEMS Microbiol. Ecol. 21 (2) (1996) 131–138, https://doi.org/10.1111/j.1574-6941.1996.tb00340.x.
[42] A.E. Giblin, C.R. Tobias, B. Song, N. Weston, G.T. Banta, V.H. Rivera-Monroy, The Importance of Dissimilatory Nitrate Reduction to Ammonium (DNRA) in the Nitrogen Cycle of Coastal Ecosystems, Oceanography 26 (3) (2013) 124–131, https://doi.org/10.5670/oceanog.2013.54.
[43] J.T. Ji, Y.Z. Peng, B. Wang, X.Y. Li, Q. Zhang, Synergistic Partial-Denitrification, Anammox, and in-situ Fermentation (SPDAF) Process for Advanced Nitrogen Removal from Domestic and Nitrate-Containing Wastewater, Environ. Sci. Technol. 54 (6) (2020) 3702–3713, https://doi.org/10.1021/acs.est.9b07928.
[44] T.X. He, D.T. Xie, J.P. Ni, Z. Li, Z.L. Li, Nitrous oxide produced directly from ammonium, nitrate and nitrite during nitrification and denitrification, J. Hazard. Mater. 388 (2020) 8, https://doi.org/10.1016/j.jhazmat.2020.122114.
[45] J.M. Kim, H.J. Lee, D.S. Lee, C.O. Jeon, Characterization of the Denitrification-Associated Phosphorus Uptake Properties of “Candidatus Accumulibacter phosphatis” Clades in Sludge Subjected to Enhanced Biological Phosphorus Removal, Appl. Environ. Microbiol. 79 (6) (2013) 1969–1979, https://doi.org/10.1128/aem.03464-12.
[46] T. Liu, X.L. He, G.Y. Jia, J.W. Xu, X. Quan, S.J. You, Simultaneous nitrification and denitrification process using novel surface-modified suspended carriers for the treatment of real domestic wastewater, Chemosphere 247 (2020) 8, https://doi.org/10.1016/j.chemosphere.2020.125831.
[47] R.C. Zhang, C. Chen, B. Shao, W. Wang, X.J. Xu, X. Zhou, Y.N. Xiang, L. Zhao, D. J. Lee, N.Q. Ren, Heterotrophic sulfide-oxidizing nitrate-reducing bacteria enables the high performance of integrated autotrophic-heterotrophic denitrification (IAHD) process under high sulfide loading, Water Res. 178 (2020) 11, https://doi.org/10.1016/j.watres.2020.115848.